SCIENCE AND TECHNOLOGY ORGANIZATION
CENTRE FOR MARITIME RESEARCH AND EXPERIMENTATION

Reprint Series CMRE-PR-2019-112

Realistic extended target model for track before detect in maritime surveillance

Borja Errasti-Alcala, Walter Fuscaldo, Paolo Braca, Gemine Vivone

June 2019

Originally published in:

Proceedings of the OCEANS 2015 MTS/IEEE Conference, 18-21 May 2015, Genoa, Italy, doi: 10.1109/OCEANS-Genova.2015.7271624

About CMRE

The Centre for Maritime Research and Experimentation (CMRE) is a world-class NATO scientific research and experimentation facility located in La Spezia, Italy.

The CMRE was established by the North Atlantic Council on 1 July 2012 as part of the NATO Science & Technology Organization. The CMRE and its predecessors have served NATO for over 50 years as the SACLANT Anti-Submarine Warfare Centre, SACLANT Undersea Research Centre, NATO Undersea Research Centre (NURC) and now as part of the Science & Technology Organization.

CMRE conducts state-of-the-art scientific research and experimentation ranging from concept development to prototype demonstration in an operational environment and has produced leaders in ocean science, modelling and simulation, acoustics and other disciplines, as well as producing critical results and understanding that have been built into the operational concepts of NATO and the nations.

CMRE conducts hands-on scientific and engineering research for the direct benefit of its NATO Customers. It operates two research vessels that enable science and technology solutions to be explored and exploited at sea. The largest of these vessels, the NRV Alliance, is a global class vessel that is acoustically extremely quiet.

CMRE is a leading example of enabling nations to work more effectively and efficiently together by prioritizing national needs, focusing on research and technology challenges, both in and out of the maritime environment, through the collective Power of its world-class scientists, engineers, and specialized laboratories in collaboration with the many partners in and out of the scientific domain.

NOTE: The CMRE Reprint series reprints papers and articles published by CMRE authors in the open literature as an effort to widely disseminate CMRE products. Users are encouraged to cite the original article where possible.

Realistic Extended Target Model for Track Before Detect in Maritime Surveillance

Borja Errasti-Alcala*, Walter Fuscaldo*†, Paolo Braca* and Gemine Vivone*
*NATO STO CMRE, La Spezia, Italy,
{Borja.Errasti,Paolo,Braca,Gemine.Vivone}@cmre.nato.int
†Department of Information, Electronics and Telecommunications Engineering
Sapienza University of Rome, Italy
fuscaldo@diet.uniroma1.it

***Abstract*—Traditional target tracking algorithms are generally fed a set of thresholded detections under the hypothesis that no more than one detection is generated by each single target. Improvements in modern radar systems have made possible to obtain high resolution data of the targets, making them occupy more than a single resolution cell, and have made necessary to use appropriate Extended Target Tracking (ETT) techniques, since the aforementioned hypothesis is no longer valid. However, these techniques do not often take into account the physical phenomena that are involved in the radar-sea-target system. This paper explores some of the effects involved in the transmission, propagation, backscattering and processing of the radar signal in a maritime environment, that have a crucial importance in ETT. A statistical model that considers the featured effects is developed and tested in a particle filter based Track before Detect (TbD) algorithm. Accounting for physical aspects, good outcomes in both kinematic (i.e. position and velocity) and size (i.e. width and length) estimation can be pointed out using real radar data acquired by a high resolution X-band Marine radar located in the Gulf of La Spezia, Italy.**

I. Introduction

Among the systems used for surveillance and vessel monitoring in short and medium ranges, radar is probably the most widespread. In recent years, the use of pulse compression techniques, such as Linear Frequency Modulated Continuous Wave (LFMCW) [1], has allowed for the proliferation of low-cost, low-power, lightweight high resolution X-band radars, as compared to the previous pulsed radars. These systems are capable of providing measurements of the backscattered energy with a very high resolution in both range and azimuth, which makes targets in the surveillance area larger than one resolution cell.

Traditional tracking methods consider that a target may generate at most one point measurement each scan. Since this assumption is no longer valid, new tracking methodologies that consider the extent of the target, known as Extended Target Tracking (ETT), have been developed. Most of these methodologies are based on Sequential Monte Carlo (SMC) methods: In [2], the extended target is considered as a set of fixed points in a target reference frame, where the probabilistic detection of these points leads to a data association problem, which is solved by means of a target's state vector augmentation with the association hypotheses. In [3], the authors propose two different methods: An interacting multiple model data augmentation technique and a modified version of the mixture Kalman filter. In both cases, the kinematics of the target and its modal state are estimated separately, providing a reasonable tradeoff between performance and computational effort. In [4], a Bayesian filter that jointly detects and estimates the parameters of an extended object is proposed. The common assumption of elliptic target extent is considered in [5], [6] where the random matrix framework is exploited. A thorough review of Monte Carlo methods for ETT is presented in [7]. Most of these techniques allow for the retrieval of information not only about the kinematics of the target, but also about its extent.

While most target tracking, including Extended Target Tracking, techniques are fed thresholded detections [8], in order to detect and track low observable targets (e.g. rubber boats, rigid hulled inflatable boats), soft detection procedures are preferable, such as Track before Detect (TbD). On the one hand, these TbD techniques have a larger computational burden, but on the other hand, no information is lost during the thresholding process. An Extended Target TbD (ET-TbD) was introduced in [9], based on a simplified target existence/absence model proposed in [10]. Typical assumptions of ETT are elliptical targets [5], [6] and exponentially distributed clutter [10], but experiments with real data have shown that such assumptions lead to an incorrect estimation of the targets' size if no other effects are taken into account.

This paper explores the physical phenomena that are involved in the acquisition of maritime targets by means of microwave radar. Most of these effects have been traditionally overlooked by the target tracking community but they can have a relevant impact on the performance of an ETT algorithm.

The remainder of this communication is organized as follows: Section II presents the radar system used to collect the real radar data. Section III presents an overview of the proposed realistic model. The integration between this model and the particle filter-based TbD algorithm is shown in Section IV. The experimental results, comparing the proposed approach with a particle filter-based TbD technique that neglects the physical phenomena introduced in Section III, are presented in Section V. Conclusions are drawn in Section VI.

II. Description of the Radar System

The Marine Radar Node (MRN) is a configurable coherent high resolution X-band marine radar, part of the CMRE owned Radar Sensor Network, a bistatic coherent radar network. It transmits a Linear Frequency Modulated Continuous Wave

(a) Map of the area in the MRN's field of view

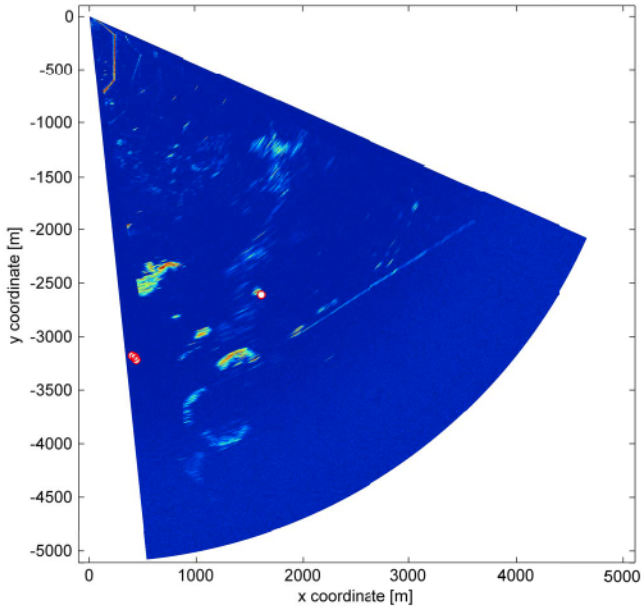

(b) One frame of the radar acquisition

Fig. 1. Maps of the area illuminated by the MRN and its corresponding acquisition. Most permanent structures can be seen in both figures. AIS reports are overprinted as white-red circles.

(LFMCW, pulse compression) [1] waveform using a narrow beam rotating antenna that works in horizontal polarization. A similar antenna acquires the received signal before it is mixed with the transmitted signal in the deramping process. The mixed signal is low-pass filtered and then sampled in an ADC process. A windowing function is applied to the digital data and a coherent High Resolution Range Profile (HRRP) is obtained as the result of the Fast Fourier Transform (FFT).

The radar's field of view is shown in Fig. 1a, while a radar acquisition is depicted in Fig. 1b. We can point out that most of the structures in the map in Fig. 1a, such as land and the breakwaters, are also visible in the radar plot in Fig. 1b.

The low complexity of the electronics and the transmission of low power, make the MRN a very compact and fast deployable system with low footprint and low probability of

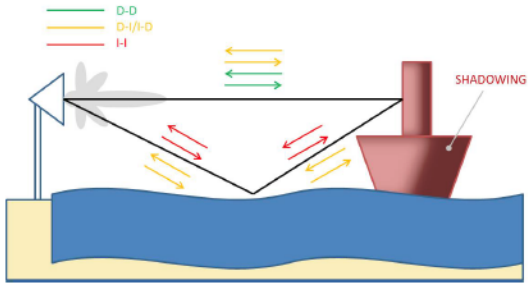

Fig. 2. Multipath and shadowing effects

intercept.

III. Overview of the Realistic Model

This section is focused on the phenomena that take place during the transmission, propagation, reflection, reception and processing of the radar signal in a maritime environment with extended targets. Some of these phenomena have a significant effect in the received signal and need to be taken into account in order to obtain accurate estimations of the targets' attributes.

A. Shadowing

The first effect to be considered is the shadowing of targets. When the wavelength of an electromagnetic wave is much smaller than the dimension of the objects involved in the propagation, the scattering phenomena are mainly governed by the laws of geometrical optics (GO) [11]. As a consequence, the scatterers of a large target that are in the radar's line of sight (LOS) create a shadow region, partially obscuring the scatterers in the occluded area. This effect, known as shadowing, is depicted in Fig. 2.

The effect of this phenomenon in the radar data is that some parts of the target appear to have a much higher reflectivity than others. In particular, scatterers at a smaller range within the same target would generate radar returns with a higher intensity than those at a larger range, since the latter are occluded by the former.

B. Multipath

Fig. 2 also shows the second effect to be considered: when GO holds, for low-grazing angles and horizontal polarization, the calm sea behaves as a quasi-perfect reflecting surface [12]. Hence, one single scatterer may produce several apparent scatterers in the radar data: one at the real range, due to the direct-direct contribution (i.e. the signal travels from the radiating system, which contains both the transmitting and receiving antennas, to the scatterer and back). A second apparent one may be found at a larger range, due to the direct-indirect (i.e. the signal goes from the radiating system to the scatterer and is reflected on the sea surface before going back) and indirect-direct (the signal is reflected on the sea surface before impinging the scatterer, from where comes back directly to the radiating system) contributions. A last apparent scatterer may appear at a larger range due to the indirect-indirect propagation. This last contribution is worth to be considered only if the reflectivity of the sea surface is very high.

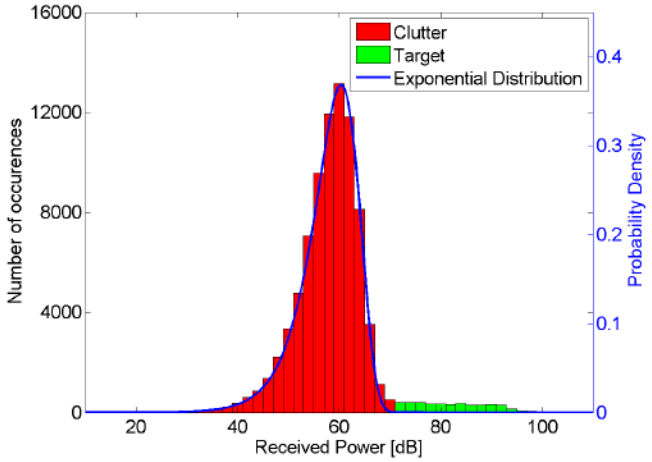

Fig. 3. Histogram of a radar acquisition with a target. The exponential distribution matches the power distribution of the clutter, but the target is not exponentially distributed. Note that the x axis of the representation is dB.

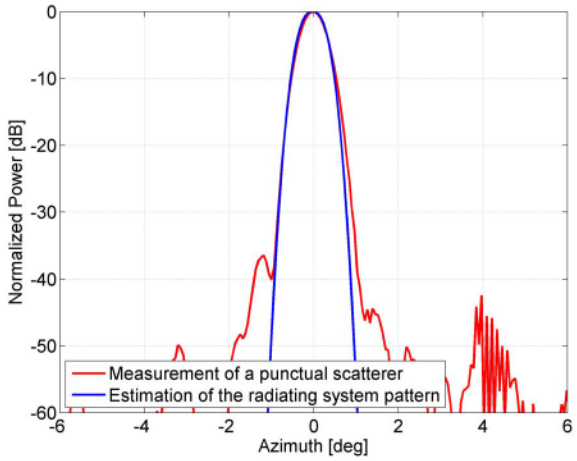

Fig. 4. Radar acquisition of a point scatterer and an approximation of the lobe shape

Since sea targets are generally complex and have multiple scatterers, the signal may be reflected an indefinite number of times before being received at the radar. However, in every reflection the signal is scattered in all the directions, hence the received power is negligible after a few bounces.

It must be considered that several scatterers at different heights are illuminated at the same time, generating replicas at different distances from the original scatterers. Consequently, the effect of the multipath phenomenon will be an enlargement of the target in the range dimension, only towards the positive range axis. This enlargement is greater for higher targets as the path difference is longer.

C. Distribution of the backscattered power

The third effect is related to the backscattered power of the target. A statistical analysis of the data shows that power of the target backscattering is not exponentially distributed, as shown in Fig. 3. Hence, a different model needs to be developed for the target, that considers the great variability of the backscattered signal inside the target introduced by various phenomena. Two of the most relevant phenomena causing this effect are the unevenness of the target's height and the possibility that a surface of the target became temporarily normal to the propagation, therefore generating a very large reflection.

D. Convolution with the antenna's radiation pattern

The fourth effect is related to the antennas' radiation pattern, that exhibit a certain lobe width. If both the transmitting and receiving antennas have a normalized gain of -10dB at $\pm 0.5°$, a single punctual scatterer will appear with an attenuation of 20dB at $\pm 0.5°$, with respect to its intensity and actual position. This effect, similar to the Point Spread Function (PSF) widely known in the optics community, is actually a convolution of the scatterers in the surveillance area with the directivity of the radiating system. The consequence of this effect, is a spread of the backscattered energy along the azimuth dimension, which leads to an overestimation of the target's size. Fig. 4 shows the radar measurement of a punctual scatterer and an estimation of the directivity of the radiating system.

The convolution with the antenna's radiation pattern has a second effect on the data that must be taken into account separately, since it affects the clutter but not the shape size of the targets. Consider that the antennas' radiation patterns have sidelobes with sidelobe levels of -15dB at $\pm 50°$ with respect to its main lobe. As the antenna rotates and illuminates a single scatterer in the FOV, the radar plot will show the scatterer's real radar return plus two replicas at the same range, but at $\pm 50°$ from its actual position, with an intensity 40dB below. Depending on the Radar Cross Section (RCS) and the range of the targets in the FOV, their replicas, i.e. ghost sidelobe targets, may be below the clutter and noise level and remain unnoticed. However, the MRN is installed in an area close to the land, which generates large radar returns that are visible even through the sidelobe. This generates a sort of *permanent clutter* in certain fixed areas of the FOV that a detection and tracking algorithm would detect as a real target. The solution for this would be to increase the threshold of the detector, if it is a individual stage of the processing chain. In a Track before Detect scenario, the solution is to discard the hypothesis that the clutter is exponentially distributed, which only holds in the area with no ghost sidelobe targets, and propose a new distribution that would take into account the possibility of having high radar returns even under the *no target* case. This effect is shown in Fig. 1, where some areas of the acquisition, e.g. Fig 1b at coordinates (2000, -1000), show a high radar return where the map, in Fig. 1a, only shows the sea surface.

E. Effect of the windowing function

This effect is related to the processing of the LFMCW waveform. For each value of the azimuth angle, after the deramping process and the low pass filtering, a Fast Fourier Transform (FFT) must be performed in order to obtain a High Resolution Range Profile (HRRP). To reduce the level of the sidelobes after the FFT the use of a window function (e.g. Hamming) is mandatory. For each scatterer, this sidelobe

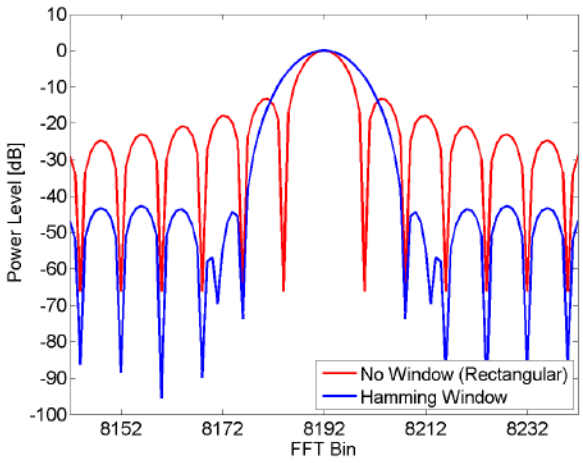

Fig. 5. Spectrum of a rectangular window and a Hamming window

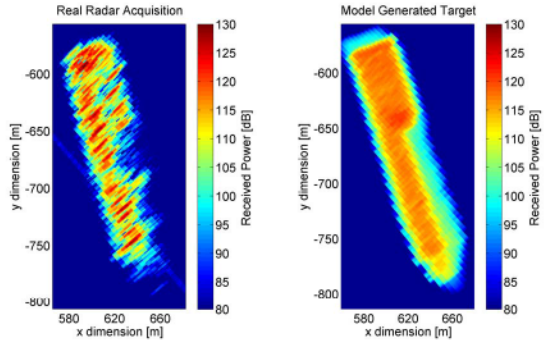

Fig. 6. Visual matching between a real acquisition of a target and its synthetic representation accounting for the discussed physical effects.

reduction comes at the cost of a widening in the size of the main lobe, as shown in Fig. 5. Therefore, a spreading effect is also present along the range dimension which, as the previous effect, leads to an overestimation of the target's size.

F. An example

Based on the real radar acquisition of a large vessel, and making use of prior knowledge about it, a synthetic radar plot has been generated that represents the same target with the consideration of the effects introduced along section III. Fig. 6 shows the real radar acquisition and the synthetic data of a 223 meter long, 28 meter wide cruise ship. Regarding the ship, generation of the synthetic data has been performed taking into account the different objects and shapes on the deck of the ship, as well as its real height and shape. Regarding the simulated radar environment, these phenomena have been considered: multipath, shadowing, windowing effect and convolution with the antennas' radiation pattern. The synthetic data has been generated in a *deterministic* way, not including of any randomness or uncertainty due to thermal noise or other effects, but rather considering only the expected value of the target's radar return in each cell. As a result, a synthetic radar target that shows a great resemblance with the real radar target is yielded.

However, the real data still show some effects, e.g. a high spatial correlation, that are not taken into account in the proposed model.

IV. Particle filter based Extended Target-Track before Detect algorithm

This section presents the particle filtering procedure used for the Extended Target Tracking-Track before Detect (ETT-TbD). The procedure considers some of the phenomena described in section III.

The objective is to sequentially estimate the probability of having a target along with its kinematics and extent (length and width). The available information is a set of raw radar frames, where each frame is a matrix of range-bearing cells that contain the measured backscattered power. Each column of this matrix is the HRRP measured at a single bearing angle.

A. Target model

Following the approach of [5], [6], where random matrices are used to model the shape of the target, an elliptic geometry is assumed here. A 6 element vector $\mathbf{x} = [x, y, \dot{x}, \dot{y}, l_1, l_2]^T$ stores the state of the targe, where (x, y) are the components of its position, $(\dot{x}, \dot{y})$ are the components of its speed and l_1 and l_2 are its length and width, respectively. The model assumes that the long axis of the ellipse, i.e. the ship's length, is parallel to its speed.

The motion of the target is considered to follow the Nearly Constant Velocity model [13]. Target dynamics are given by

$$\mathbf{x}_{n+1} = f(\mathbf{x}_n) + g(\mathbf{x}_n, \mathbf{w}_n), \tag{1}$$

$$f(\mathbf{x}_n) = \begin{bmatrix} 1 & 0 & T & 0 & 0 & 0 \\ 0 & 1 & 0 & T & 0 & 0 \\ 0 & 0 & 1 & 0 & 0 & 0 \\ 0 & 0 & 0 & 1 & 0 & 0 \\ 0 & 0 & 0 & 0 & 1 & 0 \\ 0 & 0 & 0 & 0 & 0 & 1 \end{bmatrix} \mathbf{x}_n, \tag{2}$$

$$g(\mathbf{x}_n, \mathbf{w}_n) = \begin{bmatrix} \frac{T^2}{2} & 0 & 0 & 0 \\ 0 & \frac{T^2}{2} & 0 & 0 \\ T & 0 & 0 & 0 \\ 0 & T & 0 & 0 \\ 0 & 0 & \sigma_{l_1} & 0 \\ 0 & 0 & 0 & \sigma_{l_2} \end{bmatrix} \cdot \begin{bmatrix} \sigma_{a_x} & 0 & 0 & 0 \\ 0 & \sigma_{a_y} & 0 & 0 \\ 0 & 0 & 1 & 0 \\ 0 & 0 & 0 & 1 \end{bmatrix} \mathbf{w}_n, \tag{3}$$

where T is the sampling period, σ_{l_1} and σ_{l_2} are the typical deviations of the length and width of the target respectively, $\sigma_{a_{x,y}}$ is the acceleration standard deviation along x and y, respectively. The term $\mathbf{w}_n$ indicates a four element random vector, whose elements are Gaussian distributed with zero mean and identity covariance matrix.

The presence or absence of the target is considered to follow a binary Markovian process

$$P_r(m_{n+1} = 0 \mid m_n = 0) = 1 - q_b \tag{4}$$
$$P_r(m_{n+1} = 0 \mid m_n = 1) = q_d \tag{5}$$
$$P_r(m_{n+1} = 1 \mid m_n = 0) = q_b \tag{6}$$
$$P_r(m_{n+1} = 1 \mid m_n = 1) = 1 - q_d, \tag{7}$$

where m_n is the modal state at frame n. The *no target* modal state is represented by $m_n = 0$ and the *target present* modal

state is represented by $m_n = 1$. The probabilities q_b and q_d are the probabilities of *target birth* and *target death*, respectively.

The state of the system at instant n is represented by both the modal state m_n and the vector $\mathbf{x}_n$, which is exactly the information kept by a particle. Systems of this kind are said to follow a Markovian jump model [14], [15].

B. Measurement model

The measurement model provides, for any system state (given by the modal state and vector kept in a particle), a probability distribution of the measured power in every range-bearing cell. The phenomena described in section III have an effect on this function. In order to build the measurement model, we will first consider the geometrical aspects of the radar return, and later on take the EM effects into account.

1) Target presence: The first step towards building a distribution function for the radar return in each cell, is to know in which of the acquisition cells the target is present or not. Hence, an indicator function ($\mathcal{I}$) will be built, that takes the value 1 in the cells occupied by the target, and the value 0 in the cells where only clutter is expected. This function is based on the geometrical model of the target, which, as stated before, is assumed to be elliptical.

Let (i, j) represent a single range-bearing cell of the radar acquisition, and let $[x(i,j), y(i,j)]^T$ be the vector containing its corresponding coordinates. Then, based on the elliptic geometry, we can define the indicator function ($\mathcal{I}$) as follows:

$$\mathcal{I}(i,j) = \begin{cases} 1 & \text{if} \begin{cases} \left\| N \cdot R \begin{bmatrix} x(i,j) - x \\ y(i,j) - y \end{bmatrix} \right\| < 1 \\ \text{and} \\ m = 1 \end{cases} \\ 0 & \text{otherwise} \end{cases} \tag{8}$$

where N and R are the normalization and rotation matrices, respectively

$$N = \begin{bmatrix} 2/l_1 & 0 \\ 0 & 2/l_2 \end{bmatrix} \tag{9}$$

$$R = \begin{bmatrix} \cos\phi & \sin\phi \\ -\sin\phi & \cos\phi \end{bmatrix} \tag{10}$$

and ϕ is the orientation of the target, considered parallel to its velocity:

$$\phi = \arctan\left(\frac{\dot{y}}{\dot{x}}\right). \tag{11}$$

If the indicator function $\mathcal{I}$ is computed for every range-bearing cell in the radar acquisition, the result is an *expected target map*, i.e. a matrix I with the same size as the radar acquisition, that presents the value 1 in the cells where the target is expected and value 0 where not, based on the system state.

2) Electromagnetic effects: Once the cells occupied by the target have been identified, the EM effects described in section III may be taken into account. The multipath effect, however, has a very low impact on small and medium targets for most sea conditions. Moreover, in order to model it, additional information is needed. Hence, it is disregarded here.

The phenomena introduced in section III may be divided into two groups: In the first group, those which change the behaviour of the indicator function $\mathcal{I}$ are considered: these are the windowing function and the convolution with the antennas' radiation pattern. They modify the apparent size of the target in the radar acquisition and therefore introduce a modification in the indicator function. In a second group, the phenomena that have an effect on the distribution of the radar return are considered: these are the shadowing, the variability of the backscattered power and, again, the convolution with the antennas' radiation pattern. Recall that the convolution with the antennas' radiation pattern has a twofold effect: on the one hand, it enlarges the apparent size of the targets due to the main lobe width; on the other hand, it modifies the expected radar return of the clutter due to the acquisition of real targets or land through a sidelobe.

Of course, the two groups of effects cannot be decoupled: effects in the first group do not provide a hard decision between cells that present a high radar return due to the target or a low radar return due to the clutter, but rather a smooth transition with an intermediate behaviour. This smooth transition between the target and the clutter is taken into account by a generalization of the indicator function, based on the phenomena in the first aforementioned group.

The convolution with the antennas' radiation pattern affects the acquisition by spreading the power along the azimuth dimension of the acquisition, while the windowing has an analogous effect along the range dimension. Therefore, a 2D (range-azimimuth) point spread function (PSF) may be generated using both effects, one in each dimension. Consider a column vector $\mathbf{c}$ that contains the main lobe of the FFT of a hamming window, in absolute value. Consider also a row vector $\mathbf{r}$ that contains the radiation diagram of the radiating system, as a function of the azimuth angle. The product $\mathbf{c} \cdot \mathbf{r}$ is a matrix S containing the acquisition's point spread function (PSF). For the sake of simplicity, the PSF is truncated to a dynamic range of 25dB. It must also be taken into account that the azimuth resolution of the system may be changed. Thus, the approximation in Fig. 4 is used in order to generate samples of the radiation diagram with a specific azimuth resolution. Matrix S, i.e. the system's PSF, is shown in Fig. 7.

Now we define matrix $\hat{I}$ as

$$\tilde{I} = I * S \tag{12}$$

$$\hat{I}(i,j) = \begin{cases} 1 & \text{if} \quad \tilde{I}(i,j) > 1 \\ \tilde{I}(i,j) & \text{otherwise.} \end{cases} \tag{13}$$

Matrix $\hat{I}$ is the *generalized expected target map*. It contains the value 1 in the cells where the target is present, the value 0 in the cells where only clutter may be found and, in all the other cells it contains intermediate values dictated by the influence of the target, as a consequence of the windowing and the convolution with the antennas' pattern. This matrix $\hat{I}$ will be used to interpolate between the backscattered energy distributions in the *target* and *clutter* cases: if f_T is the distribution of the radar return in a cell (i, j) such that $\mathcal{I}(i,j) = 1$, and f_C is the distribution of the radar return in a cell (i, j) such that $\mathcal{I}(i,j) = 0$, then the distribution f of

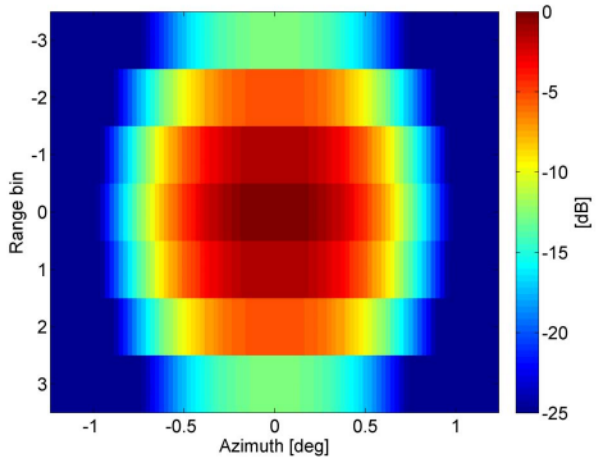

Fig. 7. The system's Point Spread Function, i.e. Matrix S

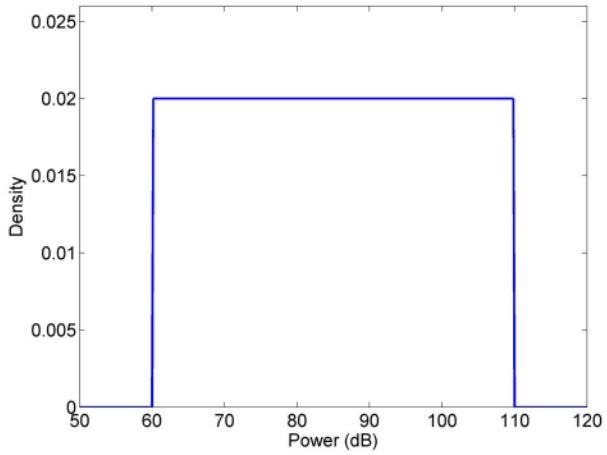

Fig. 8. Probability density uniform in the dB scale

the radar return in an arbitrary cell (i, j) is given as a convex combination of the two aforementioned distributions:

$$f = \mathcal{I}(i,j) f_T + (1 - \mathcal{I}(i,j)) f_C. \tag{14}$$

Let us now define the distribution of the radar return for the cells that contain *pure clutter* i.e. cells in which the target has no effect, and *pure target*, i.e. cells that belong to the target.

The large variability of the target's radar return must be captured with a probability density with a large support. As may be seen in Fig. 3, the distribution of the target's backscattering looks uniform in the dB scale between two certain limits. A probability density with that feature, is shown in Fig. 8, where the limits q_1 and q_2 have been set to 10^6 and 10^{11} (60dB and 110dB), respectively.

This density is defined as follows:

$$f_X^{(q_1,q_2)}(x) = \begin{cases} \frac{1}{x \log(q_2/q_1)} & \text{if} \quad q_1 < x < q_2 \\ 0 & \text{otherwise} \end{cases} \tag{15}$$

From its definition in (15), it is clear that the density has a hyperbolic shape in its support.

It is straightforward to verify that the density in Eq. (15) is well defined

$$\int_{-\infty}^{\infty} f_X^{(q_1,q_2)}(x)dx = \int_{q_1}^{q_2} \frac{1}{x \log(q_2/q_1)} dx = 1 \tag{16}$$

and that it complies with the feature of being uniform in the dB scale through the application of the random variable transformation theorem: Let Y be the random variable representing the target's backscattered power, in the dB scale. Since, $Y = g(X) = 10\log_{10}(X)$, where g is a strictly increasing continuous function, we can write

$$f_Y(y) = \begin{cases} f_X(g^{-1}(y)) |\frac{dg^{-1}(y)}{dy}| & \text{if} \quad g(q_1) < y < g(q_2) \\ 0 & \text{otherwise} \end{cases} \tag{17}$$

$$= \begin{cases} f_X(10^{\frac{y}{10}}) |\frac{10^{\frac{y}{10}} \log 10}{10}| & \text{if} \quad g(q_1) < y < g(q_2) \\ 0 & \text{otherwise} \end{cases} \tag{18}$$

$$= \begin{cases} \frac{\frac{1}{10} 10^{\frac{y}{10}} \log 10}{10^{\frac{y}{10}} \log(\frac{q_2}{q_1})} & \text{if} \quad g(q_1) < y < g(q_2) \\ 0 & \text{otherwise} \end{cases} \tag{19}$$

$$= \begin{cases} \frac{\log 10}{10 \log(\frac{q_2}{q_1})} & \text{if} \quad g(q_1) < y < g(q_2) \\ 0 & \text{otherwise} \end{cases}, \tag{20}$$

showing that the proposed density is uniform in the dB scale, between $g(q_1)$ and $g(q_2)$.

This density defines the expected backscattered energy in the cells that contain the target, and substitutes the previous exponential approach in [9]. This density accounts for the large variability of the backscattered energy due to the shadowing phenomenon and other unmodelled effects, such as e.g. specular reflections. The shadowing is considered here as independent of the view angle of the target, and assumed to affect every cell in the target in a similar way, regardless of the fact that cells at closer range may be obscuring cells at longer range, making the former show higher intensity than the latter.

The presence of a *ghost* target in the clutter suggests the use of a different clutter distribution with suitable parameters. The featured distribution presents a large support that takes into account also the different behaviour of the clutter areas contaminated by the sidelobe data from a real target or land. In such a way, the exponential model does not account for a high radar return in the clutter areas, as the new distribution does. It is worth to mention here that this new distribution is less precise for the characterization of the cells that are not contaminated with the sidelobe data.

If q_1 and q_2 were the lower and upper limits, respectively, of the proposed distribution when characterizing a target, s_1 and s_2 will be the lower and upper limits , respectively, when the distribution is used to characterize the clutter.

Summing up, we have built a method that, starting with the system state (m and $\mathbf{x}$), provides a map with the distribution of the radar return in every cell, considering the electromagnetic effects introduced in section III.

C. Likelihood function

The likelihood function $p(\mathbf{z} \mid \mathbf{x}, m)$ is based on the measurement model and assumes that cell measurements are conditionally independent. Therefore it can be computed as the product of the likelihoods of the individual cells:

$$p(\mathbf{z} \mid \mathbf{x}, m) = \prod_{(i,j)} p\left(\mathbf{z}_{(i,j)} \mid \mathbf{x}, m\right) = \\ = \prod_{(i,j)} \left(\hat{I}(i,j) f_X^{(q_1,q_2)}(\mathbf{z}_{(i,j)}) + (1 - \hat{I}(i,j)) f_X^{(s_1,qs2)}(\mathbf{z}_{(i,j)})\right) \tag{21}$$

D. Estimation procedure

We are using a Sequential Importance Resampling (SIR) particle filter. Using the statistical model defined by the likelihood (21), an approximation of the posterior distribution of the system state $(\mathbf{x}_n, m_n)$ is yielded. If N_p is the number of particles, then we have

$$p(\mathbf{x}_n, m_n \mid \mathbf{z}_1, \ldots, \mathbf{z}_n) \approx \sum_{p=1}^{N_p} w_n^{(p)} \delta_{(\mathbf{x}_n^{(p)}, m_n^{(p)})}(\mathbf{x}_n, m_n), \tag{22}$$

where

$$\left\{w_n^{(p)}, (\mathbf{x}_n^{(p)}, m_n^{(p)})\right\}_{p=1}^{N_p} \tag{23}$$

is the set of particles at time n and the factors $w^{(p)}$ are the normalized weights assigned to the particles:

$$w^{(p)} \propto p\left(\mathbf{z} \mid \mathbf{x}_n^{(p)}, m_n^{(p)}\right) \tag{24}$$

Given that (22) provides an approximation of the posterior distribution of the system state, the output of the filter, i.e. the state estimation, is computed via the MMSE estimator. Therefore, the probability of having a target is given by

$$p_n^{target} = p(m_n = 1 \mid \mathbf{z}_1, \ldots, \mathbf{z}_n) = \sum_{p=1}^{N_p} w_n^{(p)} m_n^{(p)}, \tag{25}$$

and its estimated state is given by

$$\hat{\mathbf{x}}_n = \frac{1}{p_n^{target}} \sum_{p=1}^{N_p} w_n^{(p)} m_n^{(p)} \mathbf{x}_n^{(p)}. \tag{26}$$

V. Model validation on real data

A. Radar acquisition and algorithm parameters

The realistic model described here has been applied to a real radar acquisition within the ETT-TbD framework. The exponential model used in [9] has also been executed within the same framework in order to study the effects of the phenomena described in section III. The two models were run on real radar data obtained with the system described in section II. The configuration of the radar system during the acquisition of the radar data is shown in Table I.

The parameters of the target motion model are the same for the two algorithms in order to ensure a fair comparison between them, as shown in Table II. Also, the number of particles in the filter (N_p) has been set to 1000 in both cases.

Parameter	Value
Central Frequency	9.6 GHz
Bandwidth	150 MHz
Pulse Repetition Frequency	0.978 kHz
Baseband Sampling Frequency	10 MHz
Antenna Rotation Speed	5 RPM
Period between frames (T)	12 s
Transmitted Power	24 dBm
Range Resolution	1m
Angular Precision	0.0307°
Polarization	Horizontal

TABLE I. Configuration parameters of the radar system.

Parameter	Value
p_d	10^{-6}
p_b	10^{-6}
σ_{a_x}	$10^{-2}\mathrm{m/s}^2$
σ_{a_y}	$10^{-2}\mathrm{m/s}^2$
σ_{l_1}	2m
σ_{l_2}	2m

TABLE II. Parameters of the target model

Regarding the specific parameters of the measurement models, they were set for each method, as described in Tables III and IV.

Both particle filters were pre-initialized in order to reduce its transient stage. Initial target state for the initialization was retrieved and interpolated from the AIS information transmitted by the target itself and captured by CMRE owned AIS receiver *Castellana*. The initial probability of target was set to 0.5.

The target in the radar acquisition, shown in Fig. 9, is a three masted iron-hulled barquentine with a length of 59m (LOA 69m) and a beam of 10m, used as a training vessel for the Italian Navy.

B. Results

The TbD algorithm was run with the two models and the parameters described in Section V-A, yielding the results provided in Fig. 10. The AIS information from *Castellana* sensor is included in the graphs as ground truth in order to compare the outcome of the two models.

As was already shown in [9], the exponential model is capable of discerning between the *target* and *no target* cases. In this sense, the proposed realistic model presents no differences with the exponential model, provided that both of them have yielded a posterior probability of target existence equal to 1, for all the frames in the studied radar acquisition. The different

Parameter	Value
μ_0	10^{7} (70dB)
μ_1	10^{12} (120dB)

TABLE III. Parameters of the exponential measurement model

Parameter	Value
q_1	$10^{1.5}$ (15dB)
q_2	10^{9} (90dB)
s_1	10^{5} (50dB)
s_2	10^{12} (120dB)

TABLE IV. Parameters of the hyperbolic measurement model

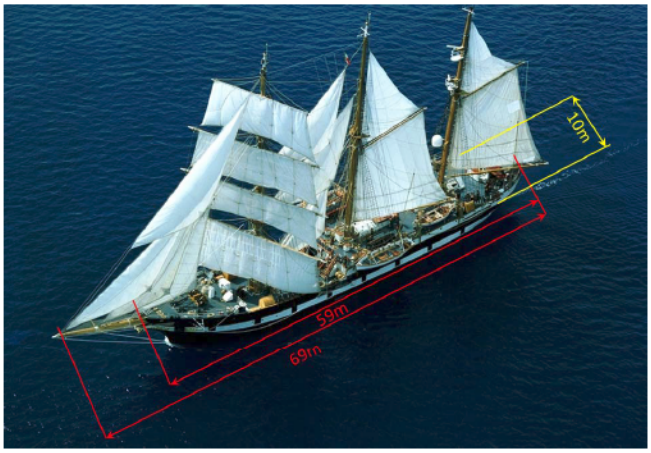

Fig. 9. The real target in the radar acquisition and its size [16].

behaviour of the models is made clear in the target parameter estimation, particularly on the target size estimation.

Indeed, it can be seen that both the exponential model and the realistic model are able to properly track the target with a very small error in position (Figs. 10a and 10b) and a relatively small error in velocity (Figs. 10c and 10d), with the realistic model yielding a slightly smaller velocity error. However, the main difference between the performance of the two models is visible in the target size estimation (Figs. 10f and 10e), where the electromagnetic effects introduced in section III have their greatest impact. The size estimation based on the realistic model is much more accurate than the exponential model's.

However, it is possible to go a little deeper in this analysis: On the one hand, the reduced noise in the velocity given by the realistic model seems to be the main contribution of using the hyperbolic target and clutter distribution, instead of the exponential one. The reason for this is that the likelihood function that results when using the hyperbolic distribution is less peaky than the one that results when using the exponential target and clutter model. The latter, tends to a particle degeneration problem that makes the filter present an oscillating behaviour with detrimental consequences for the velocity estimation. On the other hand, the higher accuracy in the size estimation provided by the realistic model, as compared to the exponential, is mainly a consequence of taking the system's point spread function into consideration. The spreading effect of the windowing process and, especially, the convolution with the antenna's radiation pattern have a conclusive effect on the target size estimation.

VI. Conclusion

A realistic target model for high resolution radar has been proposed, based on several electromagnetic effects involved in the signal transmission, propagation, backscattering and reception. Commonly overlooked effects, such as the large variability of the target's radar return due to the shadowing phenomenon, or its apparent enlargement due to the windowing process and the convolution with the antennas' radiation pattern, are now taken into consideration in this target model.

The proposed realistic model, has been integrated in a Track before Detect algorithm and it has shown to outperform the feature estimation capabilities of the former exponential model.

Acknowledgment

This work was supported by a NATO Allied Command Transformation (NATO-ACT) project on Maritime Situational Awareness (MSA).

References

[1] D. Wehner, *High resolution radar*, ser. Artech House radar library. Artech House, 1987.

[2] J. Vermaak, N. Ikoma, and S. Godsill, "Sequential monte carlo framework for extended object tracking," *Radar, Sonar and Navigation, IEE Proc.*, vol. 152, no. 5, pp. 353–363, October 2005.

[3] D. Angelova and L. Mihaylova, "Extended object tracking using monte carlo methods," *IEEE Trans. Signal Process.*, vol. 56, no. 2, pp. 825–832, Feb 2008.

[4] B. Ristic and J. Sherrah, "Particle filter for sequential detection and tracking of an extended object in clutter," in *Proc. of the* 20^{th} *Europ. Sig. Proces. Conf. (EUSIPCO)*, 2012.

[5] J. Koch, "Bayesian approach to extended object and cluster tracking using random matrices," *IEEE Trans. Aerosp. Electron. Syst.*, vol. 44, no. 3, pp. 1042–1059, July 2008.

[6] M. Feldmann, D. Franken, and W. Koch, "Tracking of extended objects and group targets using random matrices," *IEEE Trans. Signal Process.*, vol. 59, no. 4, pp. 1409–1420, April 2011.

[7] L. Mihaylova, A. Carmi, S. François, A. Gning, S. Pang, and S. Godsill, "Overview of bayesian sequential monte carlo methods for group and extended object tracking," *Digital Signal Processing*, vol. 25, pp. 1–16, 2014.

[8] G. Vivone, P. Braca, and B. Errasti-Alcala, "Extended Target Tracking Applied to X-band Marine Radar Data," in *Oceans 2015, Genova*, May 2015.

[9] B. Errasti-Alcala and P. Braca, "Track Before Detect Algorithm for Tracking Extended Targets applied to Real-World Data of X-band Marine Radar," in *Proc. of the* 17^{th} *Intern. Conf. on Inform. Fusion (FUSION)*, 2014.

[10] Y. Boers, H. Driessen, J. Torstensson, M. Trieb, R. Karlsson, and F. Gustafsson, "Track-before-detect algorithm for tracking extended targets," *Radar, Sonar and Navigation, IEE Proc.*, vol. 153, no. 4, pp. 345–351, August 2006.

[11] C. A. Balanis, *Advanced Engineering Electromagnetics*. John Wiley & Sons, 2nd Ed., 2012.

[12] J. N. Briggs, *Target Detection by Marine Radar*. Institution of Engineering & Technology, 2004.

[13] Y. Bar-Shalom, P. Willett, and X. Tian, *Tracking and Data Fusion: A Handbook of Algorithms*. Storrs, CT: YBS Publishing, 2011.

[14] S. Blackman and R. Popoli, *Design and Analysis of Modern Tracking Systems*. Artech House, 1999.

[15] Y. Bar-Shalom and X.-R. Li, *Estimation and tracking : principles, techniques, and software*. Artech House, 1993.

[16] Marina Militare. Palinuro - Classe Nave Scuola. [Online]. Available: http://www.marina.difesa.it/uominimezzi/navi/Pagine/Palinuro.aspx

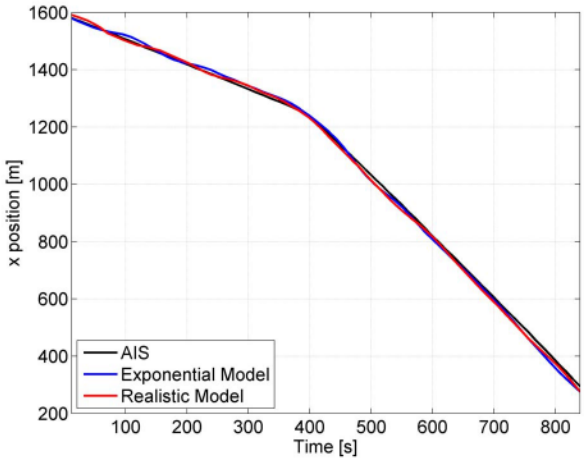

(a) Target's position, (x component)

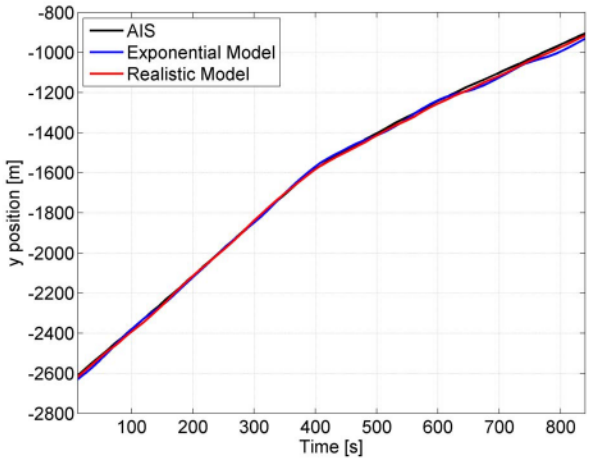

(b) Target's position, (y component)

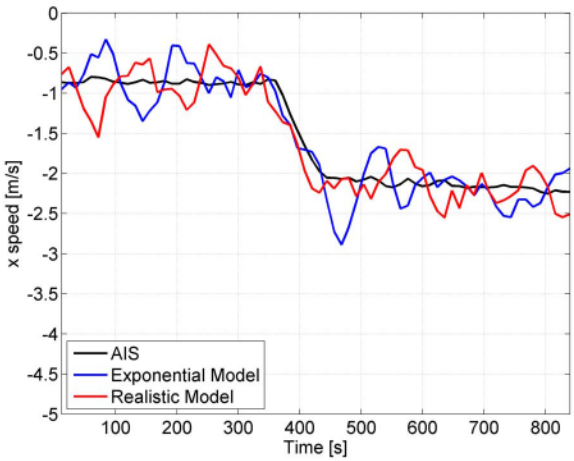

(c) Target's velocity, (x component)

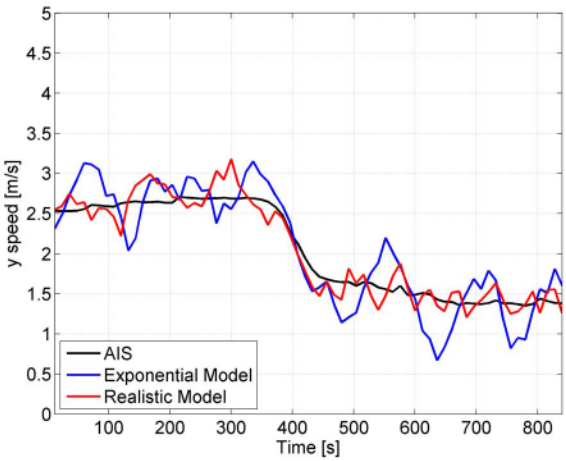

(d) Target's velocity, (y component)

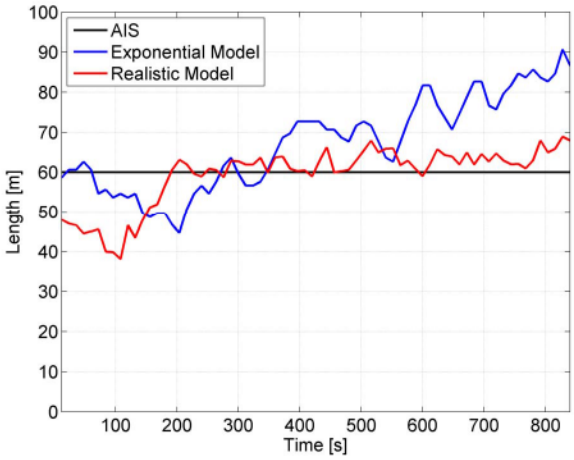

(e) Target's length

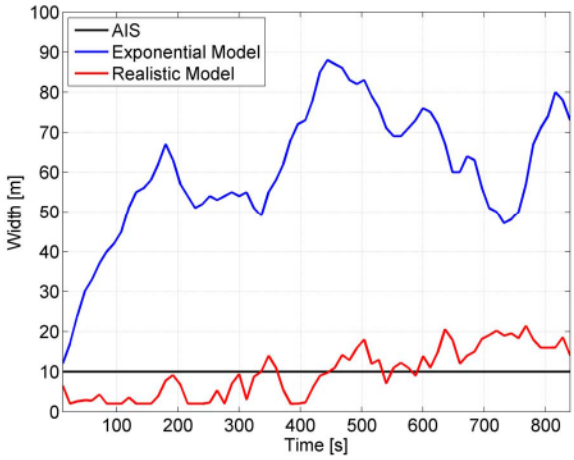

(f) Target's width

Fig. 10. Results of the compared approaches along with the AIS retrieved information

Document Data Sheet

Security Classification		Project No.
Document Serial No.	**Date of Issue**	**Total Pages**
CMRE-PR-2019-112	June 2019	9 pp.

Author(s)

Borja Errasti-Alcala, Walter Fuscaldo, Paolo Braca, Gemine Vivone

Title

Realistic extended target model for track before detect in maritime surveillance

Abstract

Traditional target tracking algorithms are generally fed a set of thresholded detections under the hypothesis that no more than one detection is generated by each single target. Improvements in modern radar systems have made possible to obtain high resolution data of the targets, making them occupy more than a single resolution cell, and have made necessary to use appropriate Extended Target Tracking (ETT) techniques, since the aforementioned hypothesis is no longer valid. However, these techniques do not often take into account the physical phenomena that are involved in the radar-sea-target system. This paper explores some of the effects involved in the transmission, propagation, backscattering and processing of the radar signal in a maritime environment, that have a crucial importance in ETT. A statistical model that considers the featured effects is developed and tested in a particle filter based Track before Detect (TbD) algorithm. Accounting for physical aspects, good outcomes in both kinematic (i.e. position and velocity) and size (i.e. width and length) estimation can be pointed out using real radar data acquired by a high resolution X-band Marine radar located in the Gulf of La Spezia, Italy.

Keywords

Radar antennas, antenna radiation patterns, target tracking, clutter, radar tracking, convolution

Issuing Organization

NATO Science and Technology Organization
Centre for Maritime Research and Experimentation

Viale San Bartolomeo 400, 19126 La Spezia, Italy

[From N. America:
STO CMRE
Unit 31318, Box 19, APO AE 09613-1318]

Tel: +39 0187 527 361
Fax:+39 0187 527 700

E-mail: library@cmre.nato.int